

Intersubband spin-density excitations in quantum wells with Rashba spin splitting

C. A. Ullrich

Department of Physics, University of Missouri-Rolla, Rolla, Missouri 65409

M. E. Flatté

Department of Physics and Astronomy, University of Iowa, Iowa City, Iowa 52242

(Dated: September 10, 2021)

In inversion-asymmetric semiconductors, spin-orbit coupling induces a \mathbf{k} -dependent spin splitting of valence and conduction bands, which is a well-known cause for spin decoherence in bulk and heterostructures. Manipulating nonequilibrium spin coherence in device applications thus requires understanding how valence and conduction band spin splitting affects carrier spin dynamics. This paper studies the relevance of this decoherence mechanism for collective intersubband spin-density excitations (SDEs) in quantum wells. A density-functional formalism for the linear spin-density matrix response is presented that describes SDEs in the conduction band of quantum wells with subbands that may be non-parabolic and spin-split due to bulk or structural inversion asymmetry (Rashba effect). As an example, we consider a 40 nm GaAs/Al_{0.3}Ga_{0.7}As quantum well, including Rashba spin splitting of the conduction subbands. We find a coupling and wavevector-dependent splitting of the longitudinal and transverse SDEs. However, decoherence of the SDEs is not determined by subband spin splitting, due to collective effects arising from dynamical exchange and correlation.

PACS numbers: 71.15.Mb; 71.45.Gm; 73.21.Fg; 72.25.Rb

I. INTRODUCTION

Most currently available semiconductor device technologies are entirely based on manipulating electronic charges. The emerging field of spintronics^{1,2} proposes to exploit, in addition, the spin degree of freedom of carriers, thereby adding new features and functionalities to solid-state devices. Many of the proposed new applications rely, in one form or another, on manipulating nonequilibrium spin coherence. The hope that this may indeed lead to viable practical approaches has been supported through recent experimental observations^{3,4,5} of long-lived (> 100 ns) and spatially extended (> 100 μm) coherent spin states in semiconductors. Two characteristic times, T_1 and T_2 , provide a quantitative measure for the magnitude and persistence of spin coherence. T_1 describes the return to equilibrium of a non-equilibrium spin population, and T_2 measures the coherence loss due to dephasing of transverse spin order (for more details, see Ref. 6).

Spin relaxation in GaAs quantum wells was recently studied experimentally^{7,8,9,10,11} and theoretically.^{12,13,14,15,16} Measurements of the electronic T_1 involve circularly polarized pump-probe techniques to create and observe coherent spin populations in the lowest conduction subband. Electron spin decoherence has been shown to occur via the spin precession¹⁷ of carriers with finite crystal momentum \mathbf{k} in the effective \mathbf{k} -dependent crystal magnetic field of an inversion-asymmetric material.¹⁸ We note that the theory of Refs. 6,15 gives good agreement with experiment, without including electron-electron interactions.

In this paper, we will consider electronic charge and spin dynamics in quantum wells involving not *one* but

two subbands (we will limit the discussion here mainly to conduction subbands). One motivation for this work is that intersubband (ISB) *charge* dynamics in quantum wells is currently of great experimental and theoretical interest,¹⁹ since electronic ISB transitions are the basis of a variety of new devices operating in the terahertz frequency regime, such as detectors,²⁰ modulators²¹ and quantum cascade lasers.^{22,23} In view of this, it seems worthwhile to explore ISB *spin* dynamics as a possible route towards novel applications in the terahertz regime.

Analogous to the case of spin dynamics discussed above, one may define characteristic times for *intersubband* dynamics (for an overview, see Ref. 24). Population decay from an excited to a lower conduction subband is measured by an intersubband relaxation time T_1^{ISB} , and loss of coherence of collective intersubband excitations is measured by a dephasing time T_2^{ISB} . These two times have been measured experimentally for ISB charge-density excitations in quantum wells^{25,26} and found to differ substantially at low temperatures, T_2^{ISB} being three orders of magnitude smaller than T_1^{ISB} . The reason is that intersubband relaxation proceeds mainly via phonon emission and is thus slowed down by an energy bottleneck for small phonon momenta as well as for the optical phonon branch. This differs from the case of conduction electron spin relaxation, where T_1 and T_2 are comparable.^{6,15}

On the other hand, dephasing of collective ISB excitations in quantum wells is determined by a complex interplay of a variety of different scattering mechanisms, whose relative importance is not *a priori* obvious. In recent experimental²⁷ and theoretical²⁸ work, it was found that the linewidth of (homogeneously broadened) ISB charge plasmons in a wide GaAs/Al_{0.3}Ga_{0.7}As quantum well, where phonon scattering plays no role, is de-

terminated mainly by interface roughness and electronic many-body effects.

The question now arises which physical mechanisms govern the dephasing of *collective* ISB spin-density excitations. As a first step towards a clarification of this question, this paper addresses the influence of the \mathbf{k} -dependent crystal magnetic field in semiconductor quantum wells on ISB spin-density excitations, and the importance of many-body effects. The latter will be described in the framework of density-functional theory (DFT).

This paper is organized as follows. In Section II we set up the formalism for calculating the electronic ground state in modulation-doped quantum well conduction subbands, including spin-orbit coupling and many-body effects. Section III presents a general response formalism for the spin-density matrix, based on time-dependent DFT (TDDFT). In Section IV we consider an explicit example and calculate the collective ISB charge- and spin-density excitations in the conduction band of a GaAs/Al_{0.3}Ga_{0.7}As quantum well, including spin-orbit coupling. Section V contains our conclusions. Various technical details can be found in Appendices A and B.

II. ELECTRONIC GROUND STATE

We consider a modulation-doped quantum well (direction of growth: z -axis) containing N conduction electrons per unit area. In the standard multi-band $\mathbf{k} \cdot \mathbf{p}$ approach for semiconductors,^{29,30,31,32} the single-particle states in a quantum well are expanded in terms of Bloch functions at the zone center, $u_n(\mathbf{r})$:

$$\Psi_{j\mathbf{q}_{||}}(\mathbf{r}) = \sum_{n=1}^{N_b} e^{i\mathbf{q}_{||}\mathbf{r}_{||}} \psi_{jn}(z) u_n(\mathbf{r}), \quad (1)$$

where $\psi_{jn}(z)$ are envelope function belonging to the j th subband, and $\mathbf{r}_{||} = (x, y)$ and $\mathbf{q}_{||} = (q_x, q_y)$ are in-plane position and wave vectors. In general, $u_n(\mathbf{r}) = u_{n\uparrow}(\mathbf{r})\xi_{\uparrow} + u_{n\downarrow}(\mathbf{r})\xi_{\downarrow}$, where $\xi_{\uparrow,\downarrow}$ denote two-component Pauli spinors. The functions $u_{n\sigma}(\mathbf{r})$ have the form $u_{n\sigma}(\mathbf{r}) = c_{n\sigma}|j\rangle$, where $c_{n\sigma}$ are complex coefficients. Usually N_b includes at least the conduction-band s states and the valence-band p states (8-band or Kane²⁹ model), but in general a 14-band model is needed for a consistent description of spin splitting in heterostructures.³³ In that case, the set of basis functions is

$$|j\rangle \in \left\{ |Z\rangle_v, |X \pm iY\rangle_v, |S\rangle_c, |Z\rangle_c, |X \pm iY\rangle_c \right\}. \quad (2)$$

This leads to a Hamiltonian in 8×8 (or 14×14) matrix form, whose elements are well known.^{30,31} The envelope functions $\psi_{jn}(z)$ for valence and conduction bands then follow from the resulting 8 (or 14) coupled single-particle equations.³⁰

If one is only interested in the electronic structure of the conduction band of a quantum well, it is convenient to reduce the multi-band Hamiltonian described above

to a 2×2 conduction band Hamiltonian.^{33,34,35,36,37} The single-particle states (1) can then be simplified to the following two-component form:

$$\Psi_{j\mathbf{q}_{||}}(\mathbf{r}) = e^{i\mathbf{q}_{||}\mathbf{r}_{||}} \begin{pmatrix} \varphi_{j\uparrow}(\mathbf{q}_{||}, z) \\ \varphi_{j\downarrow}(\mathbf{q}_{||}, z) \end{pmatrix}. \quad (3)$$

The envelope functions $\varphi_{j\sigma}$ follow from a two-component effective-mass Kohn-Sham equation:

$$\sum_{\beta=\uparrow,\downarrow} \left(\hat{h} \delta_{\alpha\beta} + v_{\alpha\beta}^{\text{ext}}(z) + \hat{H}_{\alpha\beta}^{\text{so}}(z) + v_{\alpha\beta}^{\text{xc}}(z) \right) \varphi_{j\beta}(\mathbf{q}_{||}, z) = E_{j\mathbf{q}_{||}} \varphi_{j\alpha}(\mathbf{q}_{||}, z), \quad (4)$$

where $\alpha = \uparrow, \downarrow$, and

$$\hat{h} = -\frac{d}{dz} \frac{\hbar^2}{2m(E, z)} \frac{d}{dz} + \frac{\hbar^2 q_{||}^2}{2m(E, z)} + v_{\text{conf}}(z) + v_{\text{H}}(z). \quad (5)$$

The spin-independent part \hat{h} of the 2×2 conduction band Hamiltonian accounts for possible non-parabolicity of the subbands through an effective mass that depends on $E_{j\mathbf{q}_{||}}$. Explicit expressions for $m(E, z)$ can be found in Refs. 36,37. $v_{\text{conf}}(z)$ is the confining bare quantum well potential (e.g., a square well), and the Hartree potential $v_{\text{H}}(z)$ is related to the electron ground-state density $n(z)$, defined below, through Poisson's equation:

$$\frac{d^2 v_{\text{H}}(z)}{dz^2} = -4\pi e^* n(z), \quad (6)$$

where $e^* = e/\sqrt{\epsilon}$ is the effective charge (ϵ is the static dielectric constant of the material).

Let us now discuss the spin-dependent parts of the Hamiltonian in Eq. (4). The first term, $v_{\alpha\beta}^{\text{ext}}(z)$, describes externally applied uniform static electric and magnetic fields, \mathbf{E} and \mathbf{B} :

$$v_{\alpha\beta}^{\text{ext}}(z) = eE_z z \delta_{\alpha\beta} + \frac{1}{2} g^*(z) \mu_B \mathbf{B} \cdot \vec{\sigma}, \quad (7)$$

where $\mathbf{E} = \hat{e}_z E_z$ is perpendicular to the quantum well, and \mathbf{B} can have arbitrary direction. $\vec{\sigma}$ is the vector of the Pauli spin matrices, and $g^*(z)$ denotes the g-factor of the bulk material at point z .

Intrinsic conduction band spin splitting, caused by spin-orbit interaction, in general comes from several different sources. One often deals with situation where there are two major contributions: $\hat{H}_{\alpha\beta}^{\text{so}} = \hat{H}_{\alpha\beta}^{\text{BIA}} + \hat{H}_{\alpha\beta}^{\text{SIA}}$, where BIA and SIA denote bulk and structural inversion asymmetry. The first term has the well-known form $\hat{H}_{\alpha\beta}^{\text{BIA}} = [\hbar \mathbf{\Omega} \cdot \vec{\sigma}/2]_{\alpha\beta}$, where $\mathbf{\Omega} = \gamma (q_x(q_y^2 - q_z^2), q_y(q_z^2 - q_x^2), q_z(q_x^2 - q_y^2))$ for bulk zincblende semiconductors.¹⁸

For a quantum well, $\hat{H}_{\alpha\beta}^{\text{BIA}}$ depends on the growth direction. For instance, along [001] we have

$$\begin{aligned} \hat{H}_{\uparrow\uparrow}^{\text{BIA}} &= \left(\hat{H}_{\downarrow\downarrow}^{\text{BIA}} \right)^{\dagger} = i(q_x^2 - q_y^2) \left(\frac{1}{2} \frac{d\gamma}{dz} + \gamma \frac{d}{dz} \right) \\ \hat{H}_{\uparrow\downarrow}^{\text{BIA}} &= \left(\hat{H}_{\downarrow\uparrow}^{\text{BIA}} \right)^{\dagger} = -\frac{d}{dz} \gamma \frac{d}{dz} (q_x + iq_y) \\ &\quad - i\gamma q_x q_y (q_x - iq_y), \end{aligned} \quad (8)$$

for [110] and [111] directions, see Ref. 35. The second contribution to intrinsic spin splitting, SIA (also known as the Rashba effect³⁸), has the form

$$\hat{H}_{\uparrow\uparrow}^{\text{SIA}} = \hat{H}_{\downarrow\downarrow}^{\text{SIA}} = 0 \quad (9)$$

$$\hat{H}_{\uparrow\downarrow}^{\text{SIA}} = \left(\hat{H}_{\downarrow\uparrow}^{\text{SIA}} \right)^{\dagger} = -\frac{i}{2} \frac{d\eta}{dz} (q_x - iq_y). \quad (10)$$

The material parameters $\gamma(z)$ and $\eta(z)$ are explicitly given in Ref. 37. We also mention a possible additional source of spin splitting in quantum wells, the so-called native interface asymmetry, related to chemical bonds across interfaces (for more details see Refs. 6,39).

A novel feature in Eq. (4), which distinguishes the present approach from previous studies of conduction band non-parabolicity and spin splitting, is that many-body effects are explicitly included through the exchange-correlation (xc) potential $v_{\alpha\beta}^{\text{xc}}(z)$. xc effects have previously been shown to produce non-negligible shifts of quantum well subband energies and ISB charge plasmon frequencies.^{24,28,40} As discussed below, including xc effects is crucial for a physically correct description of collective ISB spin excitations.

The solutions of Eq. (4) have the interesting property of being mixed spin-up and spin-down eigenstates, due to the off-diagonal terms in the Hamiltonian caused by spin-orbit coupling and, possibly, externally applied transverse magnetic fields. The off-diagonal terms in $\hat{H}_{\alpha\beta}^{\text{so}}$ depend on $\mathbf{q}_{||}$, and there is no choice of basis which diagonalizes Eq. (4) for *all* $\mathbf{q}_{||}$. Due to the absence of a global quantization axis, spin is no longer a good quantum number. This requires a generalization of the well-known spin-DFT⁴¹ to systems with non-collinear spin. So far, this was done at only few occasions in the literature, namely for non-collinear magnetic materials such as $\gamma\text{-Fe}$, U_3Pt_4 and Mn_3Sn ,^{42,43} and inhomogeneous quantum Hall systems,⁴⁴ but, to our knowledge, never before in the present context of semiconductor nanostructures.

Formally, the xc potential is defined as

$$v_{\alpha\beta}^{\text{xc}}(\mathbf{r}) = \frac{\delta E_{\text{xc}}[\underline{n}]}{\delta n_{\alpha\beta}(\mathbf{r})}, \quad (11)$$

where the xc energy of the system, $E_{\text{xc}}[\underline{n}]$, is a functional of the spin-density matrix⁴¹

$$\underline{n}(\mathbf{r}) = \sum_{j, \mathbf{q}_{||}} f_{j\mathbf{q}_{||}} \Psi_{j\mathbf{q}_{||}} \Psi_{j\mathbf{q}_{||}}^{\dagger} \equiv \begin{pmatrix} n_{\uparrow\uparrow} & n_{\uparrow\downarrow} \\ n_{\downarrow\uparrow} & n_{\downarrow\downarrow} \end{pmatrix}, \quad (12)$$

where $f_{j\mathbf{q}_{||}} \equiv f(E_F - E_{j\mathbf{q}_{||}})$ denotes the Fermi occupation function, and E_F is the conduction band Fermi level. For $\Psi_{j\mathbf{q}_{||}}$ given by Eq. (3), we have

$$n_{\uparrow\uparrow}(z) = \sum_{j, \mathbf{q}_{||}} f_{j\mathbf{q}_{||}} |\varphi_{j\uparrow}(\mathbf{q}_{||}, z)|^2 \quad (13)$$

[similarly for $n_{\downarrow\downarrow}(z)$], and

$$n_{\uparrow\downarrow}(z) = n_{\downarrow\uparrow}^*(z) = \sum_{j, \mathbf{q}_{||}} f_{j\mathbf{q}_{||}} \varphi_{j\uparrow}(\mathbf{q}_{||}, z) \varphi_{j\downarrow}^*(\mathbf{q}_{||}, z). \quad (14)$$

The usual approximation is to take the density matrix (12) to be locally diagonal,^{43,44} so that the LSDA for non-collinear spin reads

$$v_{\alpha\beta}^{\text{xc}}(z) = \frac{\partial}{\partial n_{\alpha\beta}} [n e_{\text{xc}}^{\text{hom}}(n, |\vec{\xi}|)] \bigg|_{\underline{n} = \underline{n}(z)}. \quad (15)$$

$e_{\text{xc}}^{\text{hom}}(n, \xi)$ is the xc energy per particle of a homogeneous electron gas of density n and spin polarization ξ , which is well known from quantum Monte Carlo calculations.⁴⁵ The local density and spin polarization are given by

$$n = \text{Tr } \underline{n} \quad (16)$$

$$\vec{\xi} = \frac{1}{n} \text{Tr } \vec{\sigma} \underline{n}. \quad (17)$$

The ground-state density is normalized as $\int dz n(z) = N$. Explicit expressions for $v_{\alpha\beta}^{\text{xc}}(z)$ are given in Appendix A. With this form for $v_{\alpha\beta}^{\text{xc}}(z)$, the 2×2 effective-mass Kohn-Sham equation (4) is now completely defined. Self-consistent solution yields a set of subbands which are occupied up to E_F .

III. LINEAR RESPONSE FORMALISM FOR THE SPIN-DENSITY MATRIX

Once the electronic ground state (characterized by a set of subband levels and wave functions) has been calculated, the next step is to consider excitations. The formal framework for describing excitations in electronic many-body systems is provided by *linear response theory*.^{46,47}

For the case where the wave functions take on a two-component form, the TDDFT linear response equation for quantum wells becomes a 2×2 matrix equation:

$$n_{\sigma\sigma'}^{(1)}(\mathbf{k}_{||}, z, \omega) = \sum_{\lambda, \lambda'=\uparrow, \downarrow} \int dz' \chi_{\sigma\sigma', \lambda\lambda'}^{\text{KS}}(\mathbf{k}_{||}, z, z', \omega) \times v_{\lambda\lambda'}^{(1)}(\mathbf{k}_{||}, z', \omega). \quad (18)$$

This expresses, formally exactly, the first-order change of the spin-density matrix, $n_{\sigma\sigma'}^{(1)}$, via the response of a non-interacting system, characterized by the response function $\chi_{\sigma\sigma', \lambda\lambda'}^{\text{KS}}$ (see below), to an effective perturbing potential of the form $v_{\lambda\lambda'}^{(1)} = v_{\lambda\lambda'}^{(1, \text{ext})} + v_{\lambda\lambda'}^{(1, \text{H})} + v_{\lambda\lambda'}^{(1, \text{xc})}$. Here, $v_{\lambda\lambda'}^{(1, \text{ext})}$ is the external perturbation, and the linearized Hartree and xc potentials are

$$\begin{aligned}
& v_{\lambda\lambda'}^{(1,\text{H})}(\mathbf{k}_{||}, z', \omega) + v_{\lambda\lambda'}^{(1,\text{xc})}(\mathbf{k}_{||}, z', \omega) \\
&= \sum_{\zeta, \zeta'=\uparrow, \downarrow} \int dz'' \left[\frac{2\pi e^{*2}}{k_{||}} e^{-k_{||}|z'-z''|} \delta_{\lambda\lambda'} \delta_{\zeta\zeta'} + f_{\lambda\lambda', \zeta\zeta'}^{\text{xc}}(\mathbf{k}_{||}, z', z'', \omega) \right] n_{\zeta\zeta'}^{(1)}(\mathbf{k}_{||}, z'', \omega). \quad (19)
\end{aligned}$$

In the widely used adiabatic local-density approximation (ALDA),⁴⁸ the xc kernel is given by

$$f_{\lambda\lambda', \zeta\zeta'}^{\text{xc}}(\mathbf{k}_{||}, z, z', \omega) = \frac{\partial^2 e_{\text{xc}}^{\text{hom}}(n, |\vec{\xi}|)}{\partial n_{\lambda\lambda'}(z) \partial n_{\zeta\zeta'}(z)} \delta(z - z'). \quad (20)$$

The non-interacting response function takes on the form of a fourth-rank tensor:

$$\underline{\underline{\chi}}^{\text{KS}}(\mathbf{r}, \mathbf{r}', \omega) = \sum_{jl}^{\infty} \sum_{\mathbf{q}_{||} \mathbf{q}'_{||}} (f_{j\mathbf{q}_{||}} - f_{l\mathbf{q}'_{||}}) \frac{\Psi_{j\mathbf{q}_{||}}(\mathbf{r}) \Psi_{l\mathbf{q}'_{||}}^{\dagger}(\mathbf{r}) \Psi_{j\mathbf{q}_{||}}^{\dagger}(\mathbf{r}') \Psi_{l\mathbf{q}'_{||}}(\mathbf{r}')}{\omega - E_{j\mathbf{q}_{||}} + E_{l\mathbf{q}'_{||}} + i\eta}, \quad (21)$$

where the Ψ 's are given by Eq. (1). Formally, this multiband response formalism describes transitions among valence and conduction subbands, as well as interband transitions. In this paper, however, we focus exclusively on intersubband transitions in the conduction band of modulation doped heterostructures. Using Eq. (3), one can then transform the response function (21) into

$$\begin{aligned}
\chi_{\sigma\sigma', \lambda\lambda'}^{\text{KS}}(\mathbf{k}_{||}, z, z', \omega) &= \sum_{jl} \int \frac{d^2 q_{||}}{(2\pi)^2} \frac{f_{l\mathbf{q}_{||}-\mathbf{k}_{||}} - f_{j\mathbf{q}_{||}}}{\omega - E_{j\mathbf{q}_{||}} + E_{l\mathbf{q}_{||}-\mathbf{k}_{||}} + i\eta} \\
&\times \varphi_{j\sigma}(\mathbf{q}_{||}, z) \varphi_{l\sigma'}^*(\mathbf{q}_{||} - \mathbf{k}_{||}, z) \varphi_{j\lambda}^*(\mathbf{q}_{||}, z') \varphi_{l\lambda'}(\mathbf{q}_{||} - \mathbf{k}_{||}, z'), \quad (22)
\end{aligned}$$

where the Kohn-Sham envelope functions $\varphi_{j\sigma}$ and energies $E_{j\mathbf{q}_{||}}$ are obtained from Eq. (4).

One can combine the perturbing spin-dependent potentials $v_{\sigma\sigma'}^{(1)}$ and the solutions $n_{\sigma\sigma'}^{(1)}$ of the response equation (18) in the following, physically more transparent way, see also Eqs. (A3) and (A4) of Appendix A:

$$V_j^{(1)} = \text{Tr} [\sigma_j \underline{v}^{(1)}] \quad (23)$$

$$m_j^{(1)} = \text{Tr} [\sigma_j \underline{n}^{(1)}], \quad (24)$$

$j = 0, 1, 2, 3$, where σ_0 is the 2×2 unit matrix, and $\sigma_1, \sigma_2, \sigma_3$ are the Pauli matrices.

$m_0^{(1)} = n_{\uparrow\uparrow}^{(1)} + n_{\downarrow\downarrow}^{(1)}$ describes a collective charge-density excitation (CDE), and $m_3^{(1)} = n_{\uparrow\uparrow}^{(1)} - n_{\downarrow\downarrow}^{(1)}$ is a longitudinal spin-density excitation (SDE) with respect to the z -axis. In terms of this choice of global spin quantization, $m_1^{(1)} = n_{\uparrow\downarrow}^{(1)} + n_{\downarrow\uparrow}^{(1)}$ and $m_2^{(1)} = i[n_{\uparrow\downarrow}^{(1)} - n_{\downarrow\uparrow}^{(1)}]$ appear as transverse spin-density (or spin-flip) excitations. The CDE couples to an oscillating electric field polarized along the z -direction, associated with $V_0^{(1)}$. The longitudinal SDE is excited by an oscillating magnetic field along z associated with $V_3^{(1)}$, and the transverse SDEs are excited by oscillating magnetic fields along x and y , associated with $V_1^{(1)}$ and $V_2^{(1)}$, respectively. We will discuss these selection rules in more detail below.

In terms of these quantities, the linear response equation (18) takes on the following form:

$$m_j^{(1)}(\mathbf{k}_{||}, z, \omega) = \sum_{k=0}^3 \int dz' \Pi_{jk}^{\text{KS}}(\mathbf{k}_{||}, z, z', \omega) V_k^{(1)}(\mathbf{k}_{||}, z', \omega). \quad (25)$$

The response functions Π_{jk}^{KS} and $\chi_{\sigma\sigma', \lambda\lambda'}^{\text{KS}}$ are related as follows:

$$\Pi_{jk}^{\text{KS}} = \sum_{\sigma, \sigma', \lambda, \lambda'} \chi_{\sigma\sigma', \lambda\lambda'}^{\text{KS}} \left(\frac{\partial m_j^{(1)}}{\partial n_{\sigma\sigma'}^{(1)}} \right) \left(\frac{\partial V_k^{(1)}}{\partial v_{\lambda\lambda'}^{(1)}} \right)^{-1}, \quad (26)$$

where the coefficients $\partial m_j^{(1)} / \partial n_{\sigma\sigma'}^{(1)} \left[= \partial V_j^{(1)} / \partial v_{\sigma\sigma'}^{(1)} \right]$ are easily obtained from Eqs. (23) or (24). Explicit expressions for Π_{jk}^{KS} are given in Appendix B. The $V_k^{(1)}$, in turn, are given as sums of external perturbations and linearized Hartree and xc terms:

$$\begin{aligned}
V_k^{(1)}(\mathbf{k}_{||}, z, \omega) &= V_k^{\text{ext}}(\mathbf{k}_{||}, z, \omega) \\
&+ \sum_{l=0}^3 \int dz' \left[\frac{2\pi e^{*2}}{k_{||}} e^{-k_{||}|z-z'|} \delta_{k0} \delta_{l0} \right. \\
&\quad \left. + f_{kl}^{\text{xc}}(\mathbf{k}_{||}, z, z', \omega) \right] m_l^{(1)}(\mathbf{k}_{||}, z', \omega). \quad (27)
\end{aligned}$$

The xc kernels f_{kl}^{xc} in ALDA are given in Appendix A.

IV. RESULTS AND DISCUSSION

A. Kohn-Sham wavefunctions and Rashba effect

We will now discuss an example to illustrate the spin-density matrix response formalism developed above. Consider the case of a 40 nm wide GaAs/Al_{0.3}Ga_{0.7}As square quantum well,^{28,40} without any externally applied static electric and magnetic fields. We make the simplifying assumption of parabolic conduction subbands (i.e., neglecting the difference of the effective masses in well and barriers). Furthermore, we neglect BIA, but assume spin splitting is dominated by SIA, described by a simplified Rashba term of the form³⁸

$$\hat{H}^{\text{SIA}} = \alpha[\vec{\sigma} \times \mathbf{q}]_z = \begin{pmatrix} 0 & R \\ R^* & 0 \end{pmatrix}, \quad (28)$$

where $R = \alpha(q_y + iq_x)$, and α is taken to be a real, positive adjustable parameter. The Rashba field is thus assumed to be the same for all conduction subbands, which is a reasonable approximation for wide quantum wells. The two-component Kohn-Sham equation (4) becomes

$$\begin{pmatrix} \hat{h}_0 + v_{\uparrow\uparrow}^{\text{xc}} & R + v_{\uparrow\uparrow}^{\text{xc}} \\ R^* + v_{\uparrow\uparrow}^{\text{xc}} & \hat{h}_0 + v_{\downarrow\downarrow}^{\text{xc}} \end{pmatrix} \begin{pmatrix} \psi_{i\uparrow} \\ \psi_{i\downarrow} \end{pmatrix} = E_{i\mathbf{q}_{||}} \begin{pmatrix} \psi_{i\uparrow} \\ \psi_{i\downarrow} \end{pmatrix}, \quad (29)$$

where $i = 1, 2, 3, \dots$, and

$$\hat{h}_0 = \frac{1}{2m^*} \left(-\frac{d^2}{dz^2} + q_{||}^2 \right) + v_{\text{conf}}(z) + v_{\text{H}}(z). \quad (30)$$

Equation (29) is solved by the following ansatz:

$$\psi_{sj\uparrow}(\mathbf{q}_{||}, z) = \frac{1}{\sqrt{2}} \varphi_j(z) \quad (31)$$

$$\psi_{sj\downarrow}(\mathbf{q}_{||}, z) = \frac{s}{\sqrt{2}} \frac{R^*}{|R|} \varphi_j(z), \quad (32)$$

where we replaced the subband index i by the pair of indices $\{sj\}$, such that $s = (-1)^i$ and $j = (i+1)/2$ for i odd and $j = i/2$ for i even. In the absence of the off-diagonal terms in Eq. (29), i.e. for inversion symmetry and hence spin degeneracy at each $\mathbf{q}_{||}$, j simply labels the spin-degenerate pairs, and s labels the members of the pairs.

It is not difficult to see that in the presence of R the ground-state density matrix remains diagonal with $n_{\uparrow\uparrow} = n_{\downarrow\downarrow}$, and hence $v_{\uparrow\uparrow}^{\text{xc}} = v_{\downarrow\downarrow}^{\text{xc}} \equiv v_{\text{xc}}$ and $v_{\uparrow\uparrow}^{\text{xc}} = v_{\downarrow\downarrow}^{\text{xc}} = 0$. The $\varphi_j(z)$ are therefore simply the solutions of the spin-unpolarized effective-mass Kohn-Sham equation

$$\left[-\frac{1}{2m^*} \frac{d^2}{dz^2} + v_{\text{conf}} + v_{\text{H}} + v_{\text{xc}} \right] \varphi_j = \epsilon_j \varphi_j, \quad (33)$$

where ϵ_j are the energy levels of the associated, doubly degenerate, parabolic subbands. The presence of the off-diagonal Rashba terms in Eq. (29), however, lifts the spin degeneracy for $\mathbf{q}_{||} \neq 0$. We thus obtain, using $|R| = \alpha q_{||}$,

$$E_{sj\mathbf{q}_{||}} = \epsilon_j + \frac{q_{||}^2}{2m^*} + s\alpha q_{||}, \quad s = \pm 1, \quad (34)$$

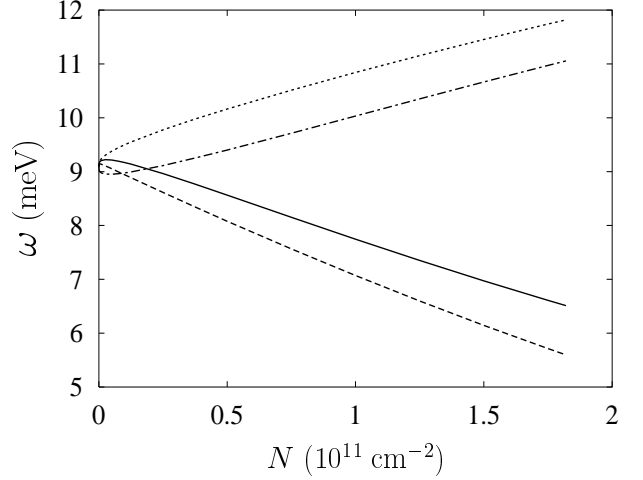


FIG. 1: Lowest (1→2) ISB excitation frequencies versus electronic sheet density N in a 40 nm GaAs/Al_{0.3}Ga_{0.7}As quantum well, at $\mathbf{k}_{||} = 0$, for values of N where only the lowest subband is occupied (with parabolic subbands and without spin-orbit splitting). Full line: single-particle excitations ($\omega = \epsilon_2 - \epsilon_1$). Dotted line: charge-density excitations in RPA. Dash-dotted and dashed lines: charge- and spin-density excitations in ALDA.

for the energy eigenvalues associated with the solutions (31),(32) of Eq. (29).

B. Collective intersubband excitations

In the following, we will consider only cases where the lowest conduction band is occupied, which restricts the electron density in the quantum well to $N < 1.82 \times 10^{11} \text{ cm}^{-2}$. The goal is to study collective charge- and spin-density excitations between the first and the second subband. These collective modes are obtained by solving the response equation (25) for the case where the external perturbation is zero. In that case, the effective perturbing potential $V_k^{(1)}$ consists of the self-consistent linearized Hartree and xc terms only.

Let us first consider the case without spin-orbit coupling ($\alpha = 0$). Figure 1 shows the density dependence of various ISB excitations at zero in-plane wavevector ($\mathbf{k}_{||} = 0$). The full line depicts the single-particle excitations with frequencies $\omega = \epsilon_2 - \epsilon_1$, i.e. the bare Kohn-Sham excitation energies. The dotted line shows the ISB charge-density excitation in RPA, i.e. setting $f_{kl}^{\text{xc}} = 0$ in the effective potential $V_k^{(1)}$, Eq. (27). The RPA excitation energies are always higher than the single-particle excitations, due to the so-called depolarization shift.⁴⁹ The ISB charge-density excitation in ALDA is shown by the dash-dotted line. Including xc effects in the response calculation produces a downshift of the plasmon energy of up to 0.75 meV. Finally, the spin-density ISB excitation is shown by the dashed line. In RPA, this excitation coincides with the single-particle excitation, since the de-

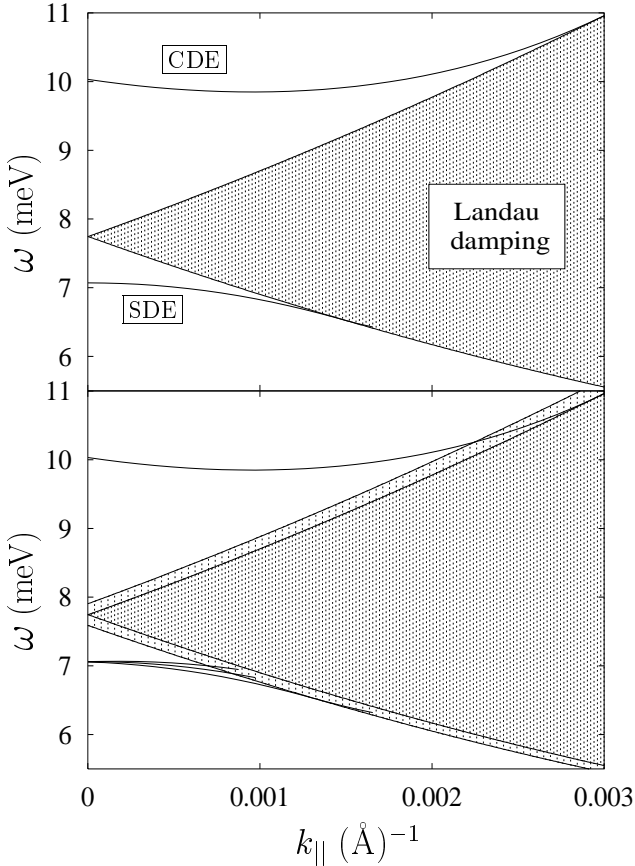


FIG. 2: ISB charge and spin plasmon wavevector dispersions in a 40 nm GaAs/Al_{0.3}Ga_{0.7}As quantum well, for Rashba coefficients $\alpha = 0$ (top) and $\alpha = 10$ meV \AA (bottom). The electronic sheet density is $1 \times 10^{11} \text{ cm}^{-2}$. The shaded regions indicate Landau damping of the charge and spin plasmons. For $\alpha = 0$, both regions coincide. For finite α , the Landau damping region for charge plasmons is unchanged (darker region), but grows for spin plasmons (darker plus lighter region). The charge plasmon is essentially independent of α , but the spin plasmon splits into three branches for finite α .

polarization shift affects only the charge mode. Thus, the spin plasmon only exists as a distinct, collective excitation because of xc effects.

We now include spin-orbit coupling in the quantum well material by taking a finite, density-independent value of $\alpha = 10$ meV \AA for the Rashba coupling parameter. This is a typical value for practical situations of interest, for instance when applying a static electric field of strength 10 kV/cm in a GaAs quantum well.³⁶

The ALDA in-plane wavevector dispersions of the ISB plasmons are shown in Figure 2, comparing the case of $\alpha = 0$ (top) and finite α (bottom). The shaded regions indicate Landau damping, i.e., collective modes overlap with the particle-hole continuum and can decay into incoherent particle-hole pairs. In both cases, the charge plasmon lies above the region of Landau damping, and the spin plasmons lie below. In the case of $\alpha = 0$, there is a common region of Landau damping for the

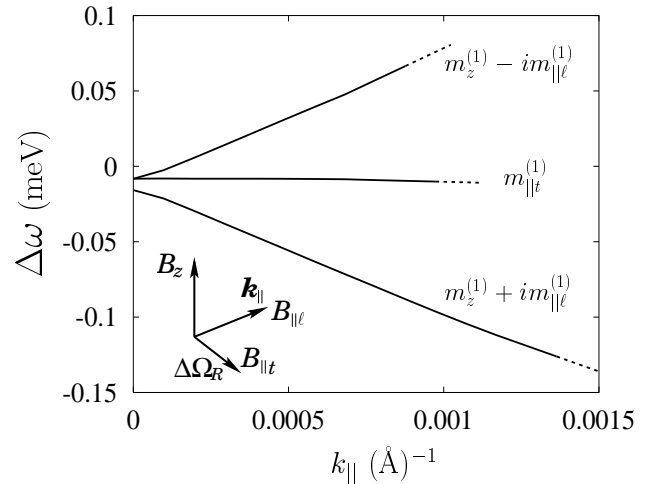


FIG. 3: Splitting of the ISB spin plasmon dispersions, for the same quantum well as in Figure 2. $\Delta\omega$ denotes the difference of the spin plasmon frequencies at $\alpha = 10$ meV \AA and $\alpha = 0$. The dots indicate that the plasmons enter the region of Landau damping. The inset illustrates the selection rules (see text). $m_z^{(1)}$ and $m_{\parallel\ell}^{(1)}$ are coupled and two-fold split. To lowest order in α , the splitting has the form $S = C(N)\alpha k_{\parallel}$, where $C(N)$ depends on the electron sheet density.

charge- and the spin plasmons. For finite α , the region of Landau damping for the spin plasmons grows, while for the charge plasmons it stays unchanged. In the absence of other intrinsic or extrinsic scattering mechanisms (phonons, disorder), all collective modes outside the region of Landau damping have infinite lifetime in ALDA.

The charge plasmon dispersion is essentially independent of α . The spin plasmon, however, splits up into three branches for finite α . This is shown in more detail in Figure 3, where $\Delta\omega$ denotes the difference of the spin plasmon frequencies at $\alpha = 10$ meV \AA and $\alpha = 0$. There are three different spin plasmon modes, all degenerate at $\alpha = 0$. We will now discuss the nature of these modes, and how they couple to external fields.

The charge and spin plasmons with $\mathbf{k}_{\parallel} = 0$ couple to external spin-dependent potentials of the form $v^{(1,\text{ext})}(z, \omega) = eE_0 z \sigma_j$. For $j = 0$ (CDE), $v^{(1,\text{ext})}$ is related to an oscillating uniform electric field $\mathbf{E} \exp(-i\omega t)$, where $\mathbf{E} = E_0 \hat{e}_z$ (linearly polarized along z , perpendicular to the quantum well plane). For the SDE's ($j = 1, 2, 3$), $v^{(1,\text{ext})}$ corresponds by comparison with Eq. (7) to oscillating magnetic fields $\mathbf{B} \exp(-i\omega t)$, where $B = 2E_0 z/g^*(z)\mu_B$. The CDE and SDE's can thus be formally viewed as collective electric and magnetic dipole transitions. At finite \mathbf{k}_{\parallel} , the plasmons couple to external potentials of the form⁵⁰ $v^{(1,\text{ext})}(\mathbf{k}_{\parallel}, z, \omega) = eE_0 a_0^* \exp(k_{\parallel} z) \sigma_j$, where a_0^* is the effective Bohr radius. As before, these potentials can be related to oscillating electric and magnetic fields, $\mathbf{E} \exp[i(\mathbf{k}_{\parallel} \cdot \mathbf{r}_{\parallel} - \omega t)]$ and $\mathbf{B} \exp[i(\mathbf{k}_{\parallel} \cdot \mathbf{r}_{\parallel} - \omega t)]$.

The inset in Figure 3 illustrates the selection rules for

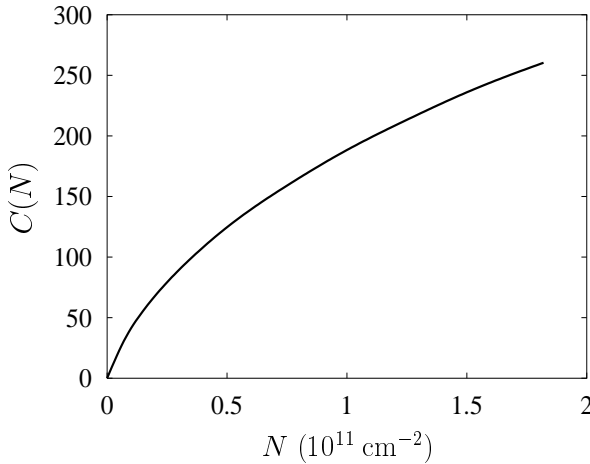


FIG. 4: ISB spin plasmon splitting coefficient $C(N)$ (see Figure 3), versus electron sheet density.

the individual SDE modes: (i) a longitudinal mode, denoted by $m_z^{(1)}$, which couples to a magnetic field perpendicular to the quantum well, $\mathbf{B} = B_z \hat{e}_z$. (ii) two transverse (or spin-flip) modes, $m_{||\ell}^{(1)}$ and $m_{||t}^{(1)}$, which couple to magnetic fields in the plane of the quantum well, $\mathbf{B} = B_{||\ell} \hat{e}_\ell$ and $\mathbf{B} = B_{||t} \hat{e}_t$, where $\hat{e}_\ell = \mathbf{k}_{||}/k_{||}$ and $\hat{e}_t = \hat{e}_\ell \times \hat{e}_z$. Figure 3 shows that, at finite α , $m_z^{(1)}$ and $m_{||\ell}^{(1)}$ are coupled and two-fold split. On the other hand, $m_{||t}^{(1)}$ depends only very little on α , except a small redshift independent of $k_{||}$. This small redshift, as well as the small splitting between the z and $||\ell$ modes at $k_{||} = 0$, can be shown to be proportional to α^2 .

Writing the Hamiltonian (28) in the form $\hat{H}^{\text{SIA}} = \hbar \Omega_R \cdot \vec{\sigma}/2$ defines the Rashba effective magnetic field $\Omega_R = (2\alpha/\hbar)(q_y, -q_x, 0)$, which lies in the quantum well plane and is perpendicular to $\mathbf{q}_{||}$. Since in our example all subbands experience the same Ω_R , a collective ISB excitation with wavevector $\mathbf{k}_{||}$ implies a change in the effective magnetic field $\Delta\Omega_R = (2\alpha/\hbar)(k_y, -k_x, 0)$ for all single-particle transitions, where $\Delta\Omega_R \parallel \hat{e}_t$ (see Figure 3). This explains the physical origin of the splitting between the different SDE branches: The two spin plasmon branches whose energies are shifted (z and $||\ell$) are those responding to fields perpendicular to $\Delta\Omega_R$, whereas the one which to lowest order in α does not shift ($||t$) is parallel to $\Delta\Omega_R$. Thus a spin polarization in either z or $||\ell$ will precess in the $z - \ell$ plane. There are two possible linear combinations, $m_z^{(1)} \pm im_{||\ell}^{(1)}$, one precessing in that direction which is favored by $\Delta\Omega_R$, the other in the opposite direction, thus costing more energy.

To lowest order in α , the magnitude of the splitting between the two linear combinations of $m_z^{(1)}$ and $m_{||\ell}^{(1)}$, S , is proportional to α and grows linearly with $k_{||}$, i.e. $S = C(N)\alpha k_{||}$. The numerical prefactor $C(N)$ is a function of the electron density, and is plotted in Figure 4. The SDE splitting strongly increases with electron density,

and reaches values of around $0.1 - 0.2$ meV for sheet densities of order $1 \times 10^{11} \text{ cm}^{-2}$ and higher, and plasmon wavevectors of order 0.001 \AA^{-1} . These splittings should be experimentally observable, for example using inelastic light scattering techniques.^{51,52} This would provide an opportunity for measuring the Rashba coefficient α .

V. CONCLUSION

We have presented a microscopic theory of collective charge- and spin-density excitations in semiconductor quantum wells based on spin-density-functional theory, with specific emphasis on intersubband excitations within the conduction band. The approach consists of two steps. We first calculate the electronic ground state in the quantum well (subband levels and envelope functions), including conduction band non-parabolicity and spin splitting, which leads to a 2×2 conduction band Hamiltonian. The associated Kohn-Sham matrix equation features spin-dependent xc potentials which are functionals of the spin-density matrix.

We then determine the excitation energies using linear response theory in the formulation of TDDFT. Formally, one needs to solve a 2×2 matrix equation for the coupled charge- and spin-density-matrix response, including dynamic many-body effects.

To illustrate the formalism, we considered the example of a quantum well with parabolic subbands that are split by a Rashba effective magnetic field. The charge plasmons were found to be independent of the Rashba field. The three possible spin plasmons, which are degenerate in the absence of spin-orbit coupling, were found to be split into three branches, the splitting being proportional to the in-plane wavevector and to the strength of the Rashba field.

This study illustrates the importance of including many-body effects beyond the RPA in calculating collective spin excitations. The collective nature of the ISB spin plasmons is purely a consequence of dynamical xc effects. Due to these collective effects, T_2^{ISB} is *not* influenced by the precessional decoherence mechanisms related to spin-orbit coupling which determine the intraband spin relaxation time T_2 .¹⁷ Therefore, in the absence of impurities, disorder and phonon scattering, the lifetime of ISB spin plasmons is limited by dynamical many-body effects only. To capture these effects, one has to go beyond the ALDA and include retardation.²⁸ Within the ALDA, on the other hand, collective CDE and SDE's are infinitely long-lived.

The effect of non-parabolic bands and more general forms of spin-orbit splitting (both BIA and SIA) in semiconductor quantum wells will be addressed in more quantitative detail in the future.

Acknowledgments

This work was supported in part by DARPA/ARO DAAD19-01-1-0490 and by the University of Missouri Research Board.

APPENDIX A: LSDA FOR NONCOLLINEAR SPINS

In LSDA,⁴¹ the xc energy per particle of a spin-polarized homogeneous electron gas, $e_{\text{xc}}^h(n, \xi)$, is usually approximated by the von Barth–Hedin parametrization:^{53,54}

$$e_{\text{xc}}^h(n, \xi) = e_{\text{xc}}^h(n, 0) + [e_{\text{xc}}^h(n, 1) - e_{\text{xc}}^h(n, 0)]f(\xi). \quad (\text{A1})$$

The interpolation function between the paramagnetic ($\xi = 0$) and ferromagnetic ($\xi = 1$) limits,

$$f(\xi) = \frac{(1 + \xi)^{4/3} + (1 - \xi)^{4/3} - 2}{2(2^{1/3} - 1)}, \quad (\text{A2})$$

reproduces the exact ξ -dependence of the exchange energy of the homogeneous electron gas, and approximates the ξ -dependence of the correlation energy.

In the LSDA for non-collinear spins,^{41,42,43,44} one still uses the spin-polarized homogeneous electron gas as reference system, assuming that the xc energy per particle depends only on the local ground-state density n and the absolute value of the local ground-state spin polarization $\vec{\xi}$, where, using definitions (16) and (17),

$$n = n_{\uparrow\uparrow} + n_{\downarrow\downarrow} \quad (\text{A3})$$

$$\vec{\xi} = \frac{1}{n} \begin{pmatrix} n_{\uparrow\downarrow} + n_{\downarrow\uparrow} \\ i(n_{\uparrow\downarrow} - n_{\downarrow\uparrow}) \\ n_{\uparrow\uparrow} - n_{\downarrow\downarrow} \end{pmatrix} \equiv \frac{1}{n} \begin{pmatrix} m_1 \\ m_2 \\ m_3 \end{pmatrix} \quad (\text{A4})$$

so that

$$|\xi| = \frac{1}{n} \sqrt{m_1^2 + m_2^2 + m_3^2}, \quad (\text{A5})$$

and the sign of ξ is determined with respect to the chosen global quantization axis: $\text{sign}(\xi) = \text{sign}(n_{\uparrow\uparrow} - n_{\downarrow\downarrow})$.

The xc potential in LSDA may then be obtained as follows: Letting $n \equiv m_0$, we define

$$v_j^{\text{xc}}(z) = \frac{\partial [ne_{\text{xc}}^h(n, \xi)]}{\partial m_j} \bigg|_{\substack{m_i = m_i(z) \\ i=0,1,2,3}} \quad (\text{A6})$$

which yields

$$v_0^{\text{xc}} = e_{\text{xc}}^h + n \frac{\partial e_{\text{xc}}^h}{\partial n} - \xi \frac{\partial e_{\text{xc}}^h}{\partial \xi} \quad (\text{A7})$$

$$v_i^{\text{xc}} = \frac{m_i}{n\xi} \frac{\partial e_{\text{xc}}^h}{\partial \xi}, \quad i = 1, 2, 3. \quad (\text{A8})$$

Using

$$v_{\alpha\beta}^{\text{xc}} = \sum_{i=0}^3 \frac{\partial m_i}{\partial n_{\alpha\beta}} v_i^{\text{xc}}, \quad \alpha, \beta = \uparrow, \downarrow, \quad (\text{A9})$$

one finds

$$v_{\uparrow\uparrow}^{\text{xc}} = e_{\text{xc}} + n \frac{\partial e_{\text{xc}}}{\partial n} + \left[\frac{n_{\uparrow\uparrow} - n_{\downarrow\downarrow}}{n\xi} - \zeta \right] \frac{\partial e_{\text{xc}}}{\partial \zeta} \quad (\text{A10})$$

$$v_{\downarrow\downarrow}^{\text{xc}} = e_{\text{xc}} + n \frac{\partial e_{\text{xc}}}{\partial n} - \left[\frac{n_{\uparrow\uparrow} - n_{\downarrow\downarrow}}{n\xi} + \zeta \right] \frac{\partial e_{\text{xc}}}{\partial \zeta} \quad (\text{A11})$$

$$v_{\uparrow\downarrow}^{\text{xc}} = \frac{2n_{\downarrow\downarrow}}{n\xi} \frac{\partial e_{\text{xc}}}{\partial \zeta} \quad (\text{A12})$$

$$v_{\downarrow\uparrow}^{\text{xc}} = \frac{2n_{\uparrow\uparrow}}{n\xi} \frac{\partial e_{\text{xc}}}{\partial \zeta}. \quad (\text{A13})$$

Equations (A10)–(A13) are in agreement with the results of Heinonen *et al.*⁴⁴

Next, we calculate, in ALDA, the xc kernels needed in Equation (27). The definition is

$$f_{jk}^{\text{xc}}(z, z', \omega) = \frac{\partial^2 [ne_{\text{xc}}^h(n, \xi)]}{\partial m_j \partial m_k} \bigg|_{\substack{m_i = m_i(z) \\ i=0,1,2,3}} \delta(z - z'), \quad (\text{A14})$$

with the following results [omitting the $\delta(z - z')$]:

$$f_{00}^{\text{xc}} = 2 \frac{\partial e_{\text{xc}}^h}{\partial n} + n \frac{\partial^2 e_{\text{xc}}^h}{\partial n^2} - 2\xi \frac{\partial^2 e_{\text{xc}}^h}{\partial n \partial \xi} + \frac{\xi^2}{n} \frac{\partial^2 e_{\text{xc}}^h}{\partial \xi^2} \quad (\text{A15})$$

$$f_{0i}^{\text{xc}} = \frac{m_i}{n\xi} \frac{\partial^2 e_{\text{xc}}^h}{\partial n \partial \xi} - \frac{m_i}{n^2} \frac{\partial^2 e_{\text{xc}}^h}{\partial \xi^2} \quad (\text{A16})$$

$$f_{ij}^{\text{xc}} = \frac{\delta_{ij}}{n\xi} \frac{\partial e_{\text{xc}}^h}{\partial \xi} - \frac{m_i m_j}{(n\xi)^3} \left(\frac{\partial e_{\text{xc}}^h}{\partial \xi} - \xi \frac{\partial^2 e_{\text{xc}}^h}{\partial \xi^2} \right), \quad (\text{A17})$$

where $i, j = 1, 2, 3$ in (A16) and (A17), and $f_{ij}^{\text{xc}} = f_{ji}^{\text{xc}}$ for all i, j . For spin unpolarized ground states ($m_1 = m_2 = m_3 = 0$), only those xc kernels diagonal in i, j are nonzero, with

$$f_{00}^{\text{xc}} = 2 \frac{\partial e_{\text{xc}}^h(n, 0)}{\partial n} + n \frac{\partial^2 e_{\text{xc}}^h(n, 0)}{\partial n^2} \quad (\text{A18})$$

and

$$f_{ii}^{\text{xc}} = \frac{4/9}{n(2^{1/3} - 1)} [e_{\text{xc}}^h(n, 1) - e_{\text{xc}}^h(n, 0)] \quad (\text{A19})$$

for $i = 1, 2, 3$. Notice that f_{00}^{xc} and f_{ii}^{xc} have the same exchange parts, $f_{00}^{\text{xc}} = f_{ii}^{\text{xc}} = (4/9n)e_{\text{xc}}^h(n, 0) = -(9\pi n^2)^{-1/3}$, but in general have different correlation parts.

APPENDIX B: NON-INTERACTING RESPONSE FUNCTIONS

For convenience, we list here the explicit relations between the response functions Π_{jk}^{KS} and $\chi_{\sigma\sigma',\lambda\lambda'}^{\text{KS}}$ following from Equations (23), (24) and (26) (omitting the superscript “KS”):

$$\begin{aligned}
\Pi_{00} &= \chi_{\uparrow\uparrow,\uparrow\uparrow} + \chi_{\uparrow\uparrow,\downarrow\downarrow} + \chi_{\downarrow\downarrow,\uparrow\uparrow} + \chi_{\downarrow\downarrow,\downarrow\downarrow} \\
\Pi_{01} &= \chi_{\uparrow\uparrow,\uparrow\downarrow} + \chi_{\uparrow\uparrow,\downarrow\uparrow} + \chi_{\downarrow\downarrow,\uparrow\downarrow} + \chi_{\downarrow\downarrow,\downarrow\uparrow} \\
\Pi_{02} &= -i(\chi_{\uparrow\uparrow,\uparrow\downarrow} - \chi_{\uparrow\uparrow,\downarrow\uparrow} + \chi_{\downarrow\downarrow,\uparrow\downarrow} - \chi_{\downarrow\downarrow,\downarrow\uparrow}) \\
\Pi_{03} &= \chi_{\uparrow\uparrow,\uparrow\uparrow} - \chi_{\uparrow\uparrow,\downarrow\downarrow} + \chi_{\downarrow\downarrow,\uparrow\uparrow} - \chi_{\downarrow\downarrow,\downarrow\downarrow} \\
\\
\Pi_{10} &= \chi_{\uparrow\downarrow,\uparrow\uparrow} + \chi_{\uparrow\downarrow,\downarrow\downarrow} + \chi_{\downarrow\uparrow,\uparrow\uparrow} + \chi_{\downarrow\uparrow,\downarrow\downarrow} \\
\Pi_{11} &= \chi_{\uparrow\downarrow,\uparrow\downarrow} + \chi_{\uparrow\downarrow,\downarrow\uparrow} + \chi_{\downarrow\uparrow,\uparrow\downarrow} + \chi_{\downarrow\uparrow,\downarrow\uparrow} \\
\Pi_{12} &= -i(\chi_{\uparrow\downarrow,\uparrow\downarrow} - \chi_{\uparrow\downarrow,\downarrow\uparrow} + \chi_{\downarrow\uparrow,\uparrow\downarrow} - \chi_{\downarrow\uparrow,\downarrow\uparrow}) \\
\Pi_{13} &= \chi_{\uparrow\downarrow,\uparrow\uparrow} - \chi_{\uparrow\downarrow,\downarrow\downarrow} + \chi_{\downarrow\uparrow,\uparrow\uparrow} - \chi_{\downarrow\uparrow,\downarrow\downarrow} \\
\\
\Pi_{20} &= i(\chi_{\uparrow\downarrow,\uparrow\uparrow} + \chi_{\uparrow\downarrow,\downarrow\downarrow} - \chi_{\downarrow\uparrow,\uparrow\uparrow} - \chi_{\downarrow\uparrow,\downarrow\downarrow}) \\
\Pi_{21} &= i(\chi_{\uparrow\downarrow,\uparrow\downarrow} + \chi_{\uparrow\downarrow,\downarrow\uparrow} - \chi_{\downarrow\uparrow,\uparrow\downarrow} - \chi_{\downarrow\uparrow,\downarrow\uparrow}) \\
\Pi_{22} &= \chi_{\uparrow\downarrow,\uparrow\uparrow} - \chi_{\uparrow\downarrow,\downarrow\downarrow} - \chi_{\downarrow\uparrow,\uparrow\uparrow} + \chi_{\downarrow\uparrow,\downarrow\downarrow} \\
\Pi_{23} &= i(\chi_{\uparrow\downarrow,\uparrow\uparrow} - \chi_{\uparrow\downarrow,\downarrow\downarrow} - \chi_{\downarrow\uparrow,\uparrow\uparrow} + \chi_{\downarrow\uparrow,\downarrow\downarrow})
\end{aligned}$$

$$\begin{aligned}
\Pi_{30} &= \chi_{\uparrow\uparrow,\uparrow\uparrow} + \chi_{\uparrow\uparrow,\downarrow\downarrow} - \chi_{\downarrow\downarrow,\uparrow\uparrow} - \chi_{\downarrow\downarrow,\downarrow\downarrow} \\
\Pi_{31} &= \chi_{\uparrow\uparrow,\uparrow\downarrow} + \chi_{\uparrow\uparrow,\downarrow\uparrow} - \chi_{\downarrow\downarrow,\uparrow\downarrow} - \chi_{\downarrow\downarrow,\downarrow\uparrow} \\
\Pi_{32} &= -i(\chi_{\uparrow\uparrow,\uparrow\downarrow} - \chi_{\uparrow\uparrow,\downarrow\uparrow} - \chi_{\downarrow\downarrow,\uparrow\downarrow} + \chi_{\downarrow\downarrow,\downarrow\uparrow}) \\
\Pi_{33} &= \chi_{\uparrow\uparrow,\uparrow\uparrow} - \chi_{\uparrow\uparrow,\downarrow\downarrow} - \chi_{\downarrow\downarrow,\uparrow\uparrow} + \chi_{\downarrow\downarrow,\downarrow\downarrow}.
\end{aligned} \tag{B1}$$

With eigenfunctions of the form (31),(32), the Kohn-Sham response function (22) can be written as

$$\begin{aligned}
\chi_{\sigma\sigma',\lambda\lambda'}^{\text{KS}}(\mathbf{k}_{||}, z, z', \omega) &= \sum_{ij} F_{\sigma\sigma',\lambda\lambda'}^{ij}(\mathbf{k}_{||}, \omega) \varphi_i(z) \varphi_j(z) \\
&\times \varphi_i(z') \varphi_j(z'),
\end{aligned} \tag{B2}$$

and likewise

$$\Pi_{kl}^{\text{KS}}(\mathbf{k}_{||}, z, z', \omega) = \sum_{ij} G_{kl}^{ij}(\mathbf{k}_{||}, \omega) \varphi_i(z) \varphi_j(z) \varphi_i(z') \varphi_j(z'). \tag{B3}$$

The $G_{kl}^{ij}(\mathbf{k}_{||}, \omega)$ are related to the $F_{\sigma\sigma',\lambda\lambda'}^{ij}(\mathbf{k}_{||}, \omega)$ according to (B1). The latter functions are given by

$$\begin{aligned}
F_{\sigma\sigma',\lambda\lambda'}^{ij}(\mathbf{k}_{||}, \omega) &= -\frac{1}{4} \sum_{ss'}^{\pm 1} \int \frac{d^2 q_{||}}{(2\pi)^2} \frac{f(E_{si\mathbf{q}_{||}})}{\omega - E_{si\mathbf{q}_{||}} + E_{s'j\mathbf{q}_{||}-\mathbf{k}_{||}} + i\eta} \left[\delta_{\sigma\uparrow} + \delta_{\sigma\downarrow} s \frac{R^*(\mathbf{q}_{||})}{|R(\mathbf{q}_{||})|} \right] \\
&\times \left[\delta_{\sigma'\uparrow} + \delta_{\sigma'\downarrow} s' \frac{R(\mathbf{q}_{||} - \mathbf{k}_{||})}{|R(\mathbf{q}_{||} - \mathbf{k}_{||})|} \right] \left[\delta_{\lambda\uparrow} + \delta_{\lambda\downarrow} s \frac{R(\mathbf{q}_{||})}{|R(\mathbf{q}_{||})|} \right] \left[\delta_{\lambda'\uparrow} + \delta_{\lambda'\downarrow} s' \frac{R^*(\mathbf{q}_{||} - \mathbf{k}_{||})}{|R(\mathbf{q}_{||} - \mathbf{k}_{||})|} \right] \\
&+ \frac{1}{4} \sum_{pp'}^{\pm 1} \int \frac{d^2 q_{||}}{(2\pi)^2} \frac{f(E_{si\mathbf{q}_{||}})}{\omega + E_{si\mathbf{q}_{||}} - E_{s'j\mathbf{q}_{||}+\mathbf{k}_{||}} + i\eta} \left[\delta_{\sigma\uparrow} + \delta_{\sigma\downarrow} s' \frac{R^*(\mathbf{q}_{||} + \mathbf{k}_{||})}{|R(\mathbf{q}_{||} + \mathbf{k}_{||})|} \right] \\
&\times \left[\delta_{\sigma'\uparrow} + \delta_{\sigma'\downarrow} s \frac{R(\mathbf{q}_{||})}{|R(\mathbf{q}_{||})|} \right] \left[\delta_{\lambda\uparrow} + \delta_{\lambda\downarrow} s' \frac{R(\mathbf{q}_{||} + \mathbf{k}_{||})}{|R(\mathbf{q}_{||} + \mathbf{k}_{||})|} \right] \left[\delta_{\lambda'\uparrow} + \delta_{\lambda'\downarrow} s \frac{R^*(\mathbf{q}_{||})}{|R(\mathbf{q}_{||})|} \right].
\end{aligned} \tag{B4}$$

It is not difficult to show that for the case of $\alpha \rightarrow 0$, i.e. vanishing Rashba term, the function $F_{\sigma\sigma',\lambda\lambda'}^{ij}$ becomes diagonal in the spin indices and reduces to the well-known limit⁴⁰ ($\omega_{ij} = \epsilon_j - \epsilon_i$)

$$F_{\sigma\sigma',\lambda\lambda'}^{ij}(\mathbf{k}_{||}, \omega) = -\delta_{\sigma\lambda} \delta_{\sigma'\lambda'} \int \frac{d^2 q_{||}}{(2\pi)^2} \left\{ \frac{f(\epsilon_i + \frac{q_{||}^2}{2m^*})}{\omega + \omega_{ij} + \frac{k_{||}^2}{2m^*} - \frac{\mathbf{q}_{||} \cdot \mathbf{k}_{||}}{m^*} + i\eta} - \frac{f(\epsilon_i + \frac{q_{||}^2}{2m^*})}{\omega - \omega_{ij} - \frac{k_{||}^2}{2m^*} - \frac{\mathbf{q}_{||} \cdot \mathbf{k}_{||}}{m^*} + i\eta} \right\}. \tag{B5}$$

¹ *Semiconductor spintronics and quantum computation*, edited by D. D. Awschalom, N. Samarth, and D. Loss (Springer, New York, 2002).

² S. A. Wolf, D. D. Awschalom, R. A. Buhrmann, J. M.

Daughton, S. von Molnàr, M. L. Roukes, A. Y. Chtchelkina, and D. M. Treger, *Science* **294**, 1488 (2001).

³ J. M. Kikkawa, I. P. Smorchkova, N. Samarth, and D. D. Awschalom, *Science* **277**, 1284 (1997).

⁴ J. M. Kikkawa and D. D. Awschalom, Phys. Rev. Lett. **80**, 4313 (1998).

⁵ J. M. Kikkawa and D. D. Awschalom, Nature **397**, 139 (1999).

⁶ M. E. Flatté, J. M. Byers, and W. H. Lau, in Ref. 1

⁷ J. Wagner, H. Schneider, D. Richards, A. Fischer, and K. Ploog, Phys. Rev. B **47**, 4786 (1993).

⁸ R. Terauchi, Y. Ohno, T. Adachi, A. Sato, F. Matsukura, A. Tackeuchi, and H. Ohno, Jpn. J. Appl. Phys. **38**, 2594 (1999).

⁹ A. Tackeuchi, O. Wada, and Y. Nishikawa, Appl. Phys. Lett. **70**, 1131 (1997); A. Tackeuchi, T. Kuroda, S. Muto, Y. Nishikawa, and O. Wada, Jpn. J. Appl. Phys. **38**, 4680 (1999).

¹⁰ Y. Ohno, R. Terauchi, T. Adachi, F. Matsukura, and H. Ohno, Phys. Rev. Lett. **83**, 4196 (1999).

¹¹ J. S. Sandhu, A. P. Heberle, J. J. Baumberg, and J. R. A. Cleaven, Phys. Rev. Lett. **86**, 2150 (2001).

¹² M. I. D'yakonov and V. Yu. Kachorovskii, Sov. Phys. Semicond. **20**, 110 (1986).

¹³ N. S. Averkiev and L. E. Golub, Phys. Rev. B **60**, 15582 (1999).

¹⁴ A. Bournel, P. Dollfus, E. Cassan, and P. Hesto, Appl. Phys. Lett. **77**, 2346 (2000).

¹⁵ W. H. Lau, J. T. Olesberg, and M. E. Flatté, Phys. Rev. B **64**, 161301 (2001).

¹⁶ W. H. Lau and M. E. Flatté, J. Appl. Phys. **91**, 8682 (2002).

¹⁷ M. I. D'yakonov and V. I. Perel', Sov. Phys. JETP **33**, 1053 (1971); Sov. Phys. Solid State **13**, 3023 (1972).

¹⁸ G. Dresselhaus, Phys. Rev. **100**, 580 (1955).

¹⁹ *Intersubband Transitions in Quantum Wells I and II*, edited by H. C. Liu and F. Capasso, Semiconductors and Semimetals Vols. 62 and 66 (Academic Press, San Diego, 2000).

²⁰ C. L. Cates, G. Briceño, M. S. Sherwin, K. D. Maranowski, K. Campman, and A. C. Gossard, Physica E **2**, 463 (1998).

²¹ P. F. Hopkins, K. L. Campman, G. Bellomi, A. C. Gossard, M. Sundaram, E. L. Yuh, and E. G. Gwinn, Appl. Phys. Lett. **64**, 348 (1994).

²² J. Faist, F. Capasso, D. L. Sivco, C. Sirtori, A. L. Hutchinson, and A. Y. Cho, Science **264**, 553 (1994).

²³ R. Köhler, A. Tredicucci, F. Beltram, H. A. Beere, E. H. Linfield, A. G. Davies, D. A. Ritchie, R. C. Iotti, and F. Rossi, Nature **417**, 156 (2002).

²⁴ M. Helm, in *Intersubband Transitions in Quantum Wells I* (Ref 19), Vol. 62, p. 1.

²⁵ J. N. Heyman, K. Unterrainer, K. Craig, B. Galdrkian, M. S. Sherwin, K. Campman, P. F. Hopkins, and A. C. Gossard, Phys. Rev. Lett. **74**, 2682 (1995).

²⁶ J. B. Williams, K. Craig, M. S. Sherwin, K. Campman, and A. C. Gossard, Physica E **2**, 177 (1998).

²⁷ J. B. Williams, M. S. Sherwin, K. D. Maranowski, and A. C. Gossard, Phys. Rev. Lett. **87**, 037401 (2001).

²⁸ C. A. Ullrich and G. Vignale, Phys. Rev. Lett. **87**, 037402 (2001).

²⁹ E. O. Kane, J. Phys. Chem. Solids **1**, 249 (1957).

³⁰ G. Bastard, *Wave mechanics applied to semiconductor heterostructures* (Halsted Press, New York, 1988).

³¹ P. Y. Yu and M. Cardona, *Fundamentals of Semiconductors* (Springer, New York, 1999).

³² F. T. Vasko and A. V. Kuznetsov, *Electronic states and optical transitions in semiconductor heterostructures* (Springer, New York, 1999).

³³ F. Malcher, G. Lommer, and U. Rössler, Superlatt. Microstruct. **2**, 267 (1986).

³⁴ R. J. Warburton, C. Gauer, A. Wixforth, J. P. Kotthaus, B. Brar, and H. Kroemer, Phys. Rev. B **53**, 7903 (1996).

³⁵ R. Eppenga and M. F. H. Schuurmans, Phys. Rev. B **37**, 10923 (1988).

³⁶ E. A. de Andrade e Silva, G. C. La Rocca, and F. Bassani, Phys. Rev. B **50**, 8523 (1994).

³⁷ P. Pfeffer and W. Zawadzki, Phys. Rev. B **59**, R5312 (1999).

³⁸ Yu. L. Bychkov and E. I. Rashba, J. Phys. C **17**, 6039 (1984).

³⁹ J. T. Olesberg, W. H. Lau, M. E. Flatté, C. Yu, E. Altunkaya, E. M. Shaw, T. C. Hasenberg, and T. F. Boggess, Phys. Rev. B **64**, 201301 (2001).

⁴⁰ C. A. Ullrich and G. Vignale, Phys. Rev. B **58**, 15756 (1999).

⁴¹ O. Gunnarsson and B. I. Lundqvist, Phys. Rev. B **13**, 4274 (1976).

⁴² J. Sticht, K. H. Höck, and J. Kübler, J. Phys.: Condens. Matter **1**, 8155 (1989).

⁴³ L. M. Sandratskii, Adv. Phys. **47**, 91 (1998).

⁴⁴ O. Heinonen, J. M. Kinaret, and M. D. Johnson, Phys. Rev. B **59**, 9073 (1999).

⁴⁵ S. H. Vosko, L. Wilk, and M. Nusair, Can. J. Phys. **58**, 1200 (1980).

⁴⁶ E. K. U. Gross and W. Kohn, Phys. Rev. Lett. **55**, 2850 (1985).

⁴⁷ M. Petersilka, U. J. Gossmann, and E. K. U. Gross, Phys. Rev. Lett. **76**, 1212 (1996).

⁴⁸ A. Zangwill and P. Soven, Phys. Rev. A **21**, 1561 (1980).

⁴⁹ S. J. Allen, D. C. Tsui, and B. Vinter, Solid State Commun. **20**, 425 (1976).

⁵⁰ A scalar external potential of this form has been used to simulate the near field of a grating coupler excited with normal-incident IR radiation, see P. R. Pinsukanjana, E. G. Gwinn, J. F. Dobson, E. L. Yuh, N. G. Asmar, M. Sundaram, and A. C. Gossard, Phys. Rev. B **46**, 7284 (1992) and J. F. Dobson, Phys. Rev. B **46**, 10163 (1992).

⁵¹ G. Abstreiter, M. Cardona, and A. Pinczuk, in *Light Scattering in Solids IV*, edited by M. Cardona and G. Güntherod, Topics in Applied Physics Vol. 54 (Springer, Berlin, 1984), p. 5.

⁵² A. Pinczuk, S. Schmitt-Rink, G. Danan, J. P. Valladares, L. N. Pfeiffer, and K. W. West, Phys. Rev. Lett. **63**, 1633 (1989).

⁵³ U. von Barth and L. Hedin, J. Phys. C **5**, 1629 (1972).

⁵⁴ R. M. Dreizler and E. K. U. Gross, *Density Functional Theory* (Springer, Berlin, 1990).